Table S1. Grid showing the cation-oxygen bonding in the majorite structure.

Atom	Mg1 (VIII)	Mg2 (VIII)	Mg3 (VII)	Si1 (IV)	Si2 (IV)	Si3 (IV)	Si4 (VI)
O1	**X**	**XX**	**XX**			**X**	
O2	**X**	**XX**				**X**	**XX**
O3	**X X**					**X**	**XX**
O4	**X X**		**XX**			**X**	
O5	**X**	**XX**	**XX**	**XXXX**			
O6	**X**	**XX**			**XXXX**		**XX**

Table S2. Optimized atomic coordinates for tetragonal $MgSiO_3$ majorite at 0 GPa compared to published experimental and computational data. The static lattice energy calculation (SLEC) results were both obtained using essentially the same potential models, except for changes to the truncation of the Buckingham potentials and the inclusion of a fourth-order spring constant in the shell model. The density functional theory (DFT) calculations were performed within the generalized gradient approximation (GGA) using VASP (this study) and CASTEP (Vinograd et al. 2006). Atoms at special positions (Mg3, Si1, S2, and Si4) are omitted from the comparison. The crystallographic origin has been shifted by 0.5, 0.0, 0.0 relative to the standard origin for space group no. 88 ($I4_1/a$). The x-ray diffraction (XRD) data were collected at ambient conditions and the uncertainties are in parentheses.

Atomic coordinates			*XRD*[a]	*SLEC* This Study	*SLEC*[b]	*DFT-GGA* This Study	*DFT-GGA*[b]
Atom	*Site*						
Mg1	D1	x	0.1253(4)	0.1261	0.1256	0.1288	0.1287
		y	0.0112(4)	0.0129	0.0120	0.0134	0.0135
		z	0.2857(3)	0.2645	0.2623	0.2663	0.2665
Mg2	D2	x	0.0000	0.0000	0.0000	0.0000	0.0000
		y	0.2500	0.2500	0.2500	0.2500	0.2500
		z	0.6258(6)	0.6229	0.6227	0.6234	0.6235
Si3	T3	x	0.1249(3)	0.1260	0.1261	0.1256	0.1254
		y	0.0065(3)	0.0115	0.0116	0.0107	0.0116
		z	0.7544(3)	0.7564	0.7560	0.7568	0.7568
O1	O(1)	x	0.0282(6)	0.0267	0.0257	0.0260	0.0268
		y	0.0550(6)	0.0591	0.0603	0.0580	0.0588
		z	0.6633(6)	0.6693	0.6685	0.6691	0.6691
O2	O(2)	x	0.0380(6)	0.0433	0.0429	0.0451	0.0447
		y	0.9529(6)	0.9559	0.9540	0.9550	0.9565
		z	0.8562(6)	0.8612	0.8610	0.8616	0.8611
O3	O(3)	x	0.2195(7)	0.2243	0.2248	0.2244	0.2234
		y	0.1023(6)	0.1075	0.1079	0.1060	0.1069
		z	0.8021(6)	0.8050	0.8070	0.8061	0.8053
O4	O(4)	x	0.2150(6)	0.2133	0.2145	0.2128	0.2117
		y	0.9106(6)	0.9166	0.9161	0.9154	0.9165
		z	0.7000(6)	0.7024	0.7013	0.7026	0.7028
O5	O(5)	x	0.9412(6)	0.9358	0.9353	0.9363	0.9372
		y	0.1617(6)	0.1639	0.1629	0.1641	0.1638
		z	0.4680(6)	0.4682	0.4690	0.4688	0.4678
O6	O(6)	x	0.8960(6)	0.8978	0.8980	0.8974	0.8977
		y	0.2080(6)	0.2128	0.2102	0.2149	0.2153
		z	0.7851(6)	0.7829	0.7821	0.7830	0.7833

[a]Angel et al. (1989); [b]Vinograd et al. (2006)

Table S3. Structure and bulk modulus of mineral phases in the Mg-Si-Al-O-H system using force fields compared to experimental results. The experimental structural results are from ambient conditions with the exception of the kaolinite data that were acquired at T = 1.5 K. The reported experimental uncertainties are in parentheses. The experimental lattice parameters of superhydrous B are based on the average of the measurements reported by Litasov et al. (2007), weighted according to the uncertainties. The experimental bulk moduli values are either Hill-averages of ambient condition elasticity measurements or are from Birch-Murnaghan equation of state measurements where K_0' = 4.

Phase		*a* (Å)	*b* (Å)	*c* (Å)	*V* (Å^3)	*α* (°)	*β* (°)	*γ* (°)	K_0 (GPa)
Pyrope	Calc.	11.462	-	-	1505.69	90.0	-	-	174.1
	Exp.[a,b]	11.4482(2)	-	-	1500.43(8)	90.0	-	-	171.2(20)
MgO	Calc.	4.205	-	-	74.33	90.0	-	-	192.9
	Exp.[c,b]	4.215(1)	-	-	74.698(3)	90.0	-	-	163.2(10)
Brucite	Calc.	3.129	-	4.823	40.88	90.0	-	120.0	35.1
	Exp.[d]	3.14(1)	-	4.76(1)	40.8(1)	90.0	-	120.0	46(1)
Quartz	Calc.	4.994	-	5.498	118.77	90.0	-	120.0	45.5
	Exp.[e,f]	4.91300(11)	-	5.40482(17)	112.981(2)	90.0	-	120.0	40.4(33)
Coesite	Calc.	7.138	12.389	7.194	547.45	90.0	120.62	90.0	115.5
	Exp.[g,h]	7.1366(2)	12.3723(4)	7.1749(3)	546.80(3)	90.0	120.33	90.0	113.7(-)
Stishovite	Calc.	4.135	-	2.722	46.54	90.0	-	-	337.5
	Exp.[i,j]	4.17755(16)	-	2.66518(34)	46.5126(61)	90.0	-	-	305(5)
Lizardite	Calc.	5.326	-	7.191	176.67	90.0	-	120.0	56.8
	Exp.[k]	5.335(5)	-	7.243(5)	178.4(5)	90.0	-	120.0	57.0(-)
Superhydrous B	Calc.	5.090	13.966	8.695	618.16	90.0	-	-	157.7
	Exp.[l,m]	5.105	14.006	8.718	623.38(39)	90.0	-	-	154.0(42)
Kaolinite	Calc.	5.194	9.076	7.401	337.95	90.04	104.35	88.99	53.2
	Exp.[n,o]	5.1535(3)	8.9419(5)	7.3906(4)	328.70(5)	91.93	104.86	89.80	47.9(8)
Corundum	Calc.	4.786	-	13.056	259.03	90.0	-	120.0	277.7
	Exp[p]	4.7617(9)	-	12.9947(17)	255.05(7)	90.0	-	120.0	257(6)

[a]Zou et al. (2012); [b]Sinogeiken and Bass (2000); [c]Jacobsen et al. (2002); [d]Xia et al. (1998); [e]Angel et al. (1997); [f]Bass et al. (1981); [g]Angel et al. (2001); [h]Weidner and Carleton (1977); [i]Andrault et al. (2003); [j]Li et al. (1996); [k]Mellini and Zanazzi. (1989); [l]Litasov et al. (2007); [m]Pacalo and Weidner (1996); [n]Bish (1993); [o]Wang et al. (2001); [p]Finger and Hazen (1978)

Figure S1. (a) Calculated pressure-volume curve for majorite using interatomic potentials from Table 1 compared to experimental values. The volume is normalized to the zero-pressure value (V_0). Based on fitting our calculated *P-V* data to the 2rd-order Birch-Murnaghan equation of state (BM-EOS), the isothermal bulk modulus (K_0) is 170.48(7) GPa. Our bulk modulus is 6% greater than that determined by the high-*P* XRD study of Yagi et al. (1992) ($P = 0 – 10$ GPa), $K_0 = 161(4)$. A 3rd-order fit of our calculated *P-V* data to the BM-EOS with K_0 fixed to 169.3 (Table 3) results in the pressure derivative $K' = 4.15$. A 3rd-order BM-EOS fit with no fixed parameters results in K_0 =169.06(2) and $K' = 4.18$. (b) Pressure dependence of the calculated axial ratio (c/a) of majorite using the potentials from Table 1 compared to experimental values. Assuming a linear relationship from $P = 0$ to $P = 10$ GPa, these results have a smaller $d(c/a)/dP = 8 \times 10^{-5}$ GPa^{-1} than experimental $d(c/a)/dP = 1.4 \times 10^{-4}$ GPa^{-1} (Yagi et al. 1992).

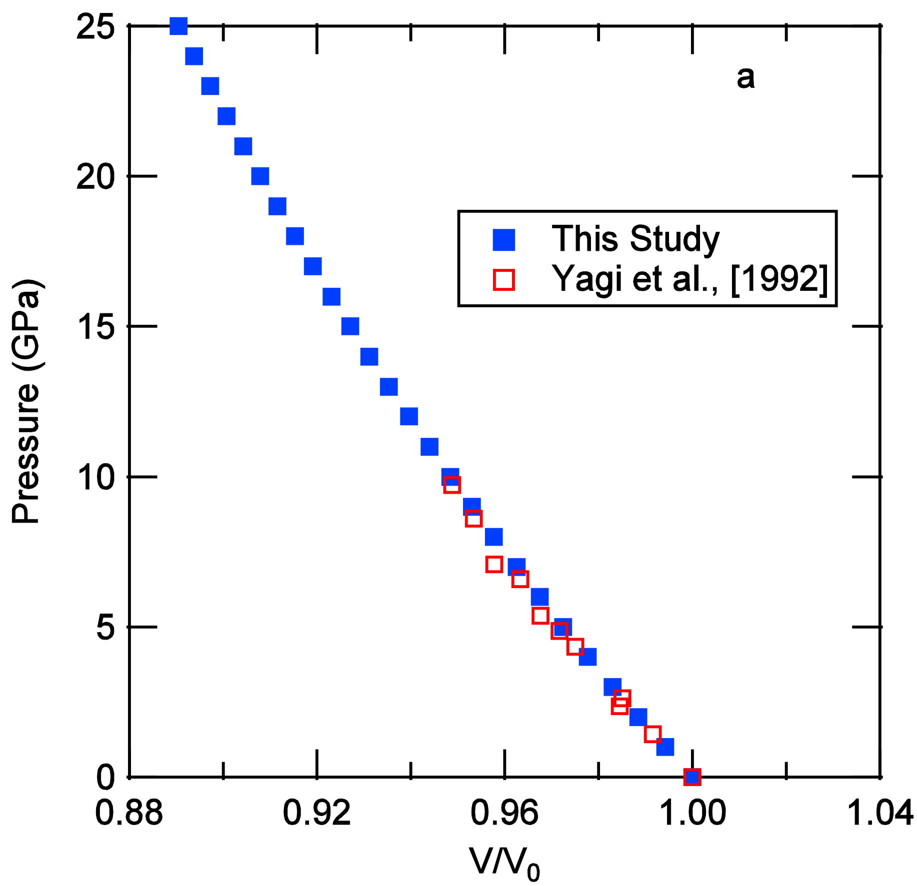

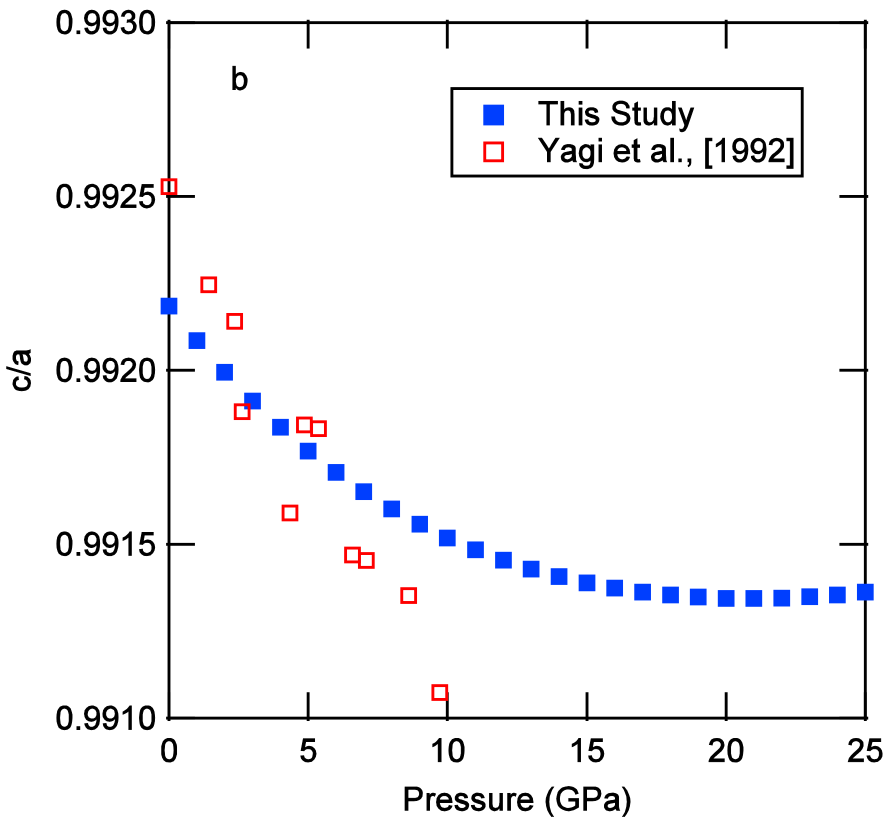
b
This Study
Yagi et al., [1992]
c/a
0.9930
0.9925
0.9920
0.9915
0.9910
0
5
10
15
20
25
Pressure (GPa)

Figure S2. Calculated pressure-volume curve for superhydrous B using the interatomic potentials in Table 1 compared to experimental multi-anvil cell (MAC) values. The bulk modulus determined by our zero-pressure calculations (K_0 = 157.7 GPa) is consistent with the value obtained through fitting our calculated *P*-*V* data with the 3rd-order BM-EOS (K_0 = 160.8(1) GPa and K_0' = 4 (fixed)). If we fix K_0 = 157.7 GPa, the result is K_0' = 4.39. Fitting for both the bulk modulus and its pressure derivative results in K_0 = 158.07(3) and K_0' = 4.35. Our bulk modulus is ~10% greater than the MAC experiments ((K_0 = 146.7(5) GPa and K_0' = 4 (fixed)).

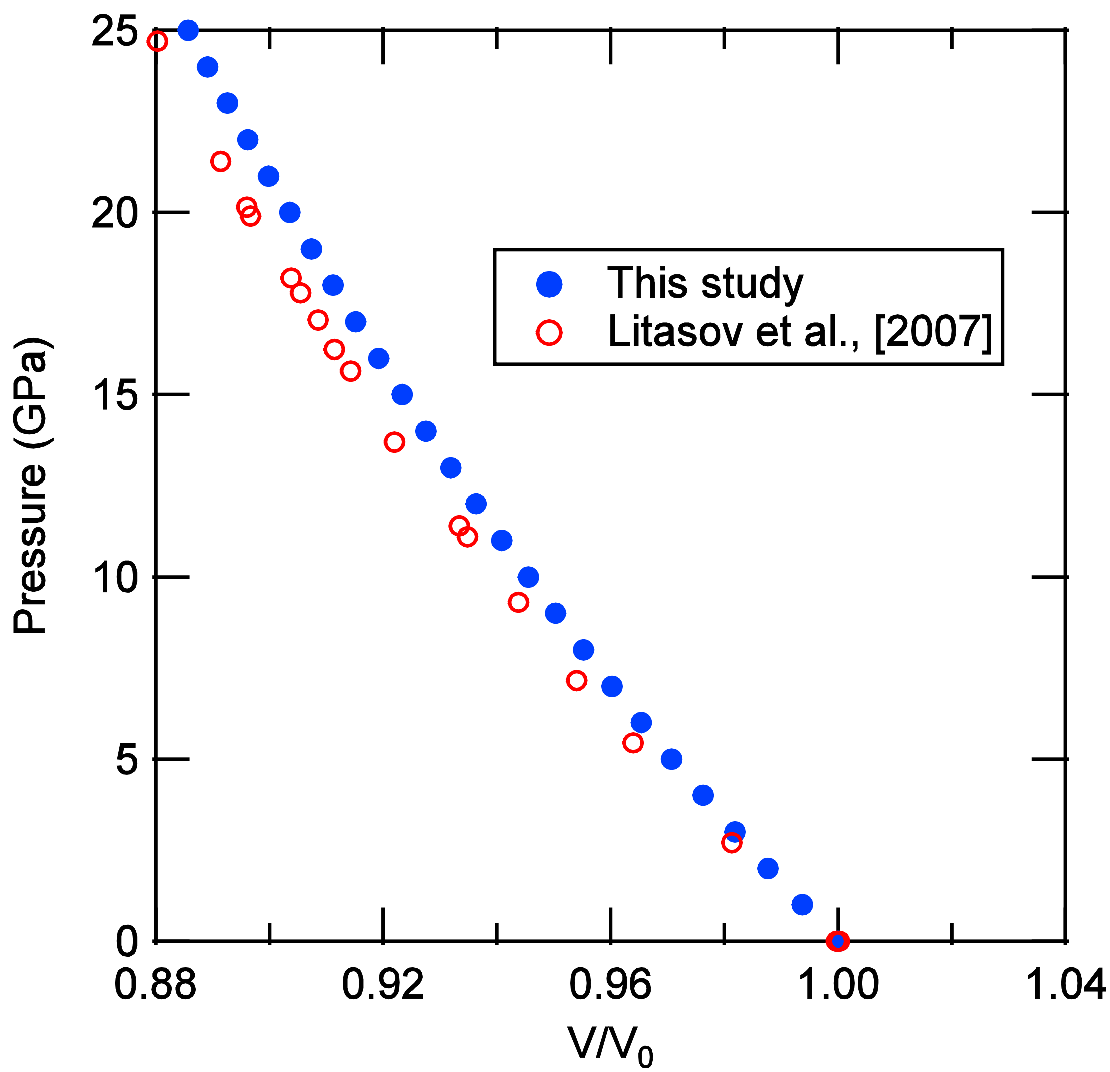

Figure S3. Calculated majorite vacancy formation enthalpies using the force fields. (a) Enthalpy associated with forming charged defects by creating Mg (circles) and Si (squares) vacancies at the ^{IV}Si1 (open blue), ^{IV}Si2 (filled red), ^{IV}Si3 (open red), ^{VI}Si4 (filled blue), ^{VIII}Mg1 (open green), ^{VIII}Mg2 (filled green), and ^{VI}Mg3 (filled blue) sites. (b) Enthalpy associated with generating an oxygen vacancy.

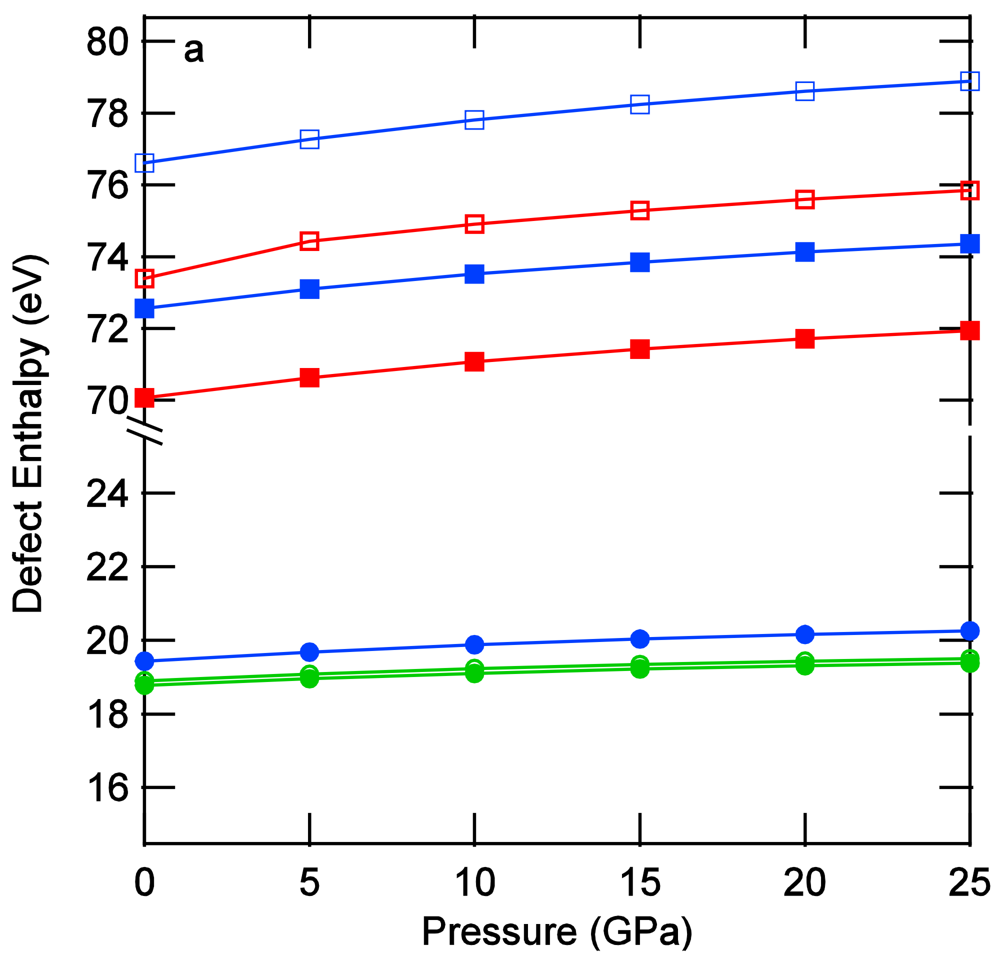

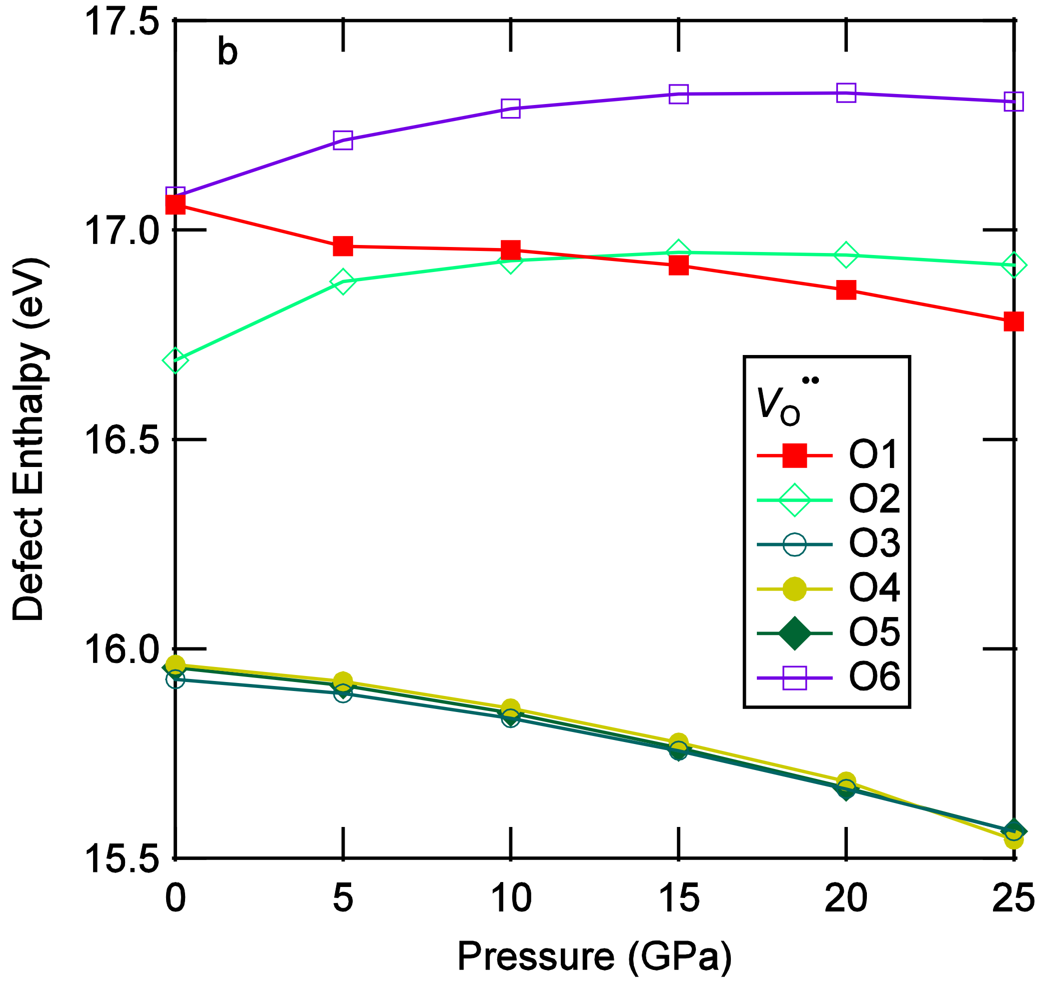
b
$V_O^{\bullet\bullet}$
O1
O2
O3
O4
O5
O6
17.5
17.0
16.5
16.0
15.5
Defect Enthalpy (eV)
0
5
10
15
20
25
Pressure (GPa)

Figure S4. Calculated defect-formation enthalpies using force fields for OH-defect complexes shown in Figure 3. Open symbols represent calculations using a 2 x 2 x 2 supercell, and the filled symbols represent calculations using the 160-atom unit cell. (a) Hydrogen incorporation via Mg vacancies. (b) Hydrogen incorporation via Si vacancies.

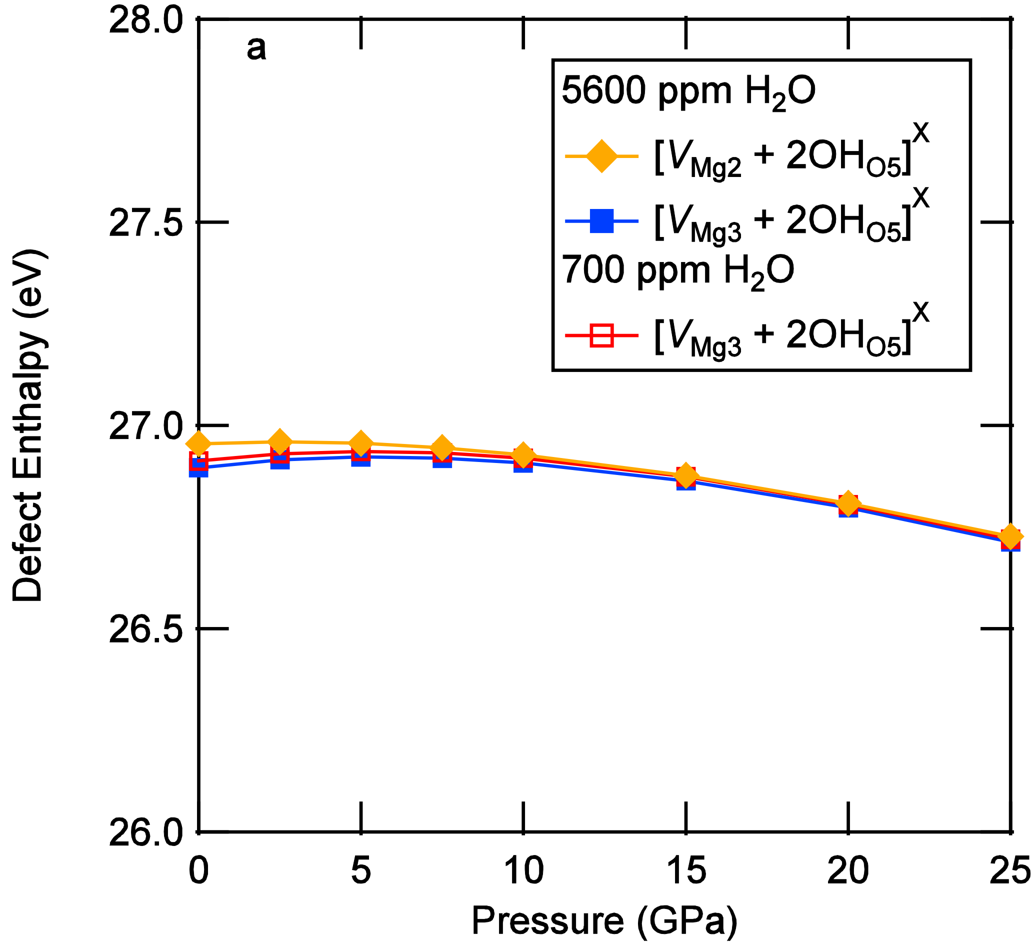

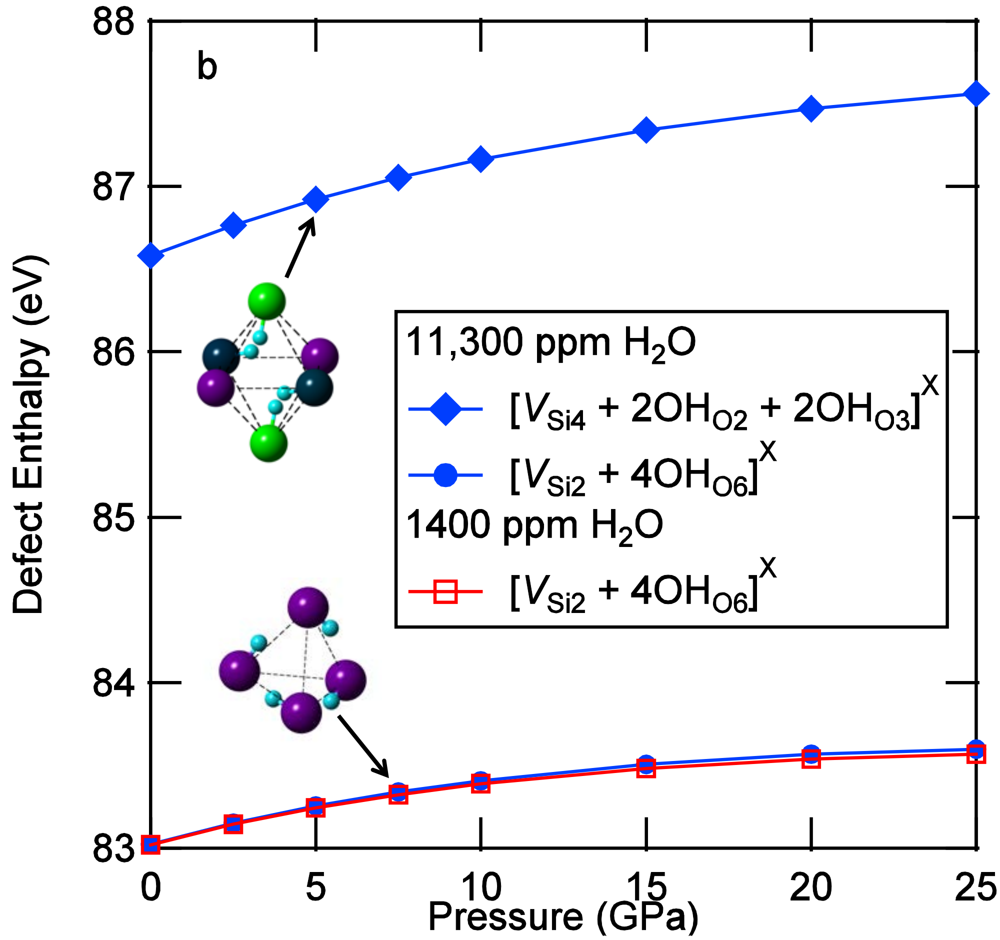
b
Defect Enthalpy (eV)
Pressure (GPa)
88
87
86
85
84
83
0
5
10
15
20
25
11,300 ppm H2O
[VSi4 + 2OHO2 + 2OHO3]X
[VSi2 + 4OHO6]X
1400 ppm H2O
[VSi2 + 4OHO6]X

References

Andrault, D., Angel, R.J., Mosenfelder, J.L., and Le Bihan, T. (2003) Equation of state of stishovite to lower mantle pressures, American Mineralogist, 88, 301-307.

Angel, R.J., Finger, L.W., Hazen, R.M., Kanzaki, M., Weidner, D.J., Liebermann, R.C. and Veblen, D.R. (1989) Structure and twinning of single-crystal $MgSiO_3$ garnet synthesized at 17 GPa and 1800 °C. American Mineralogist, 74, 509-512.

Angel. R.J., Allan, D.R., Miletich, R., and Finger, L.W. (1997) The use of quartz as an internal pressure standard in high-pressure crystallography. Journal of Applied Crytallography, 30, 461-466.

Angel, R.J., Mosenfelder, J.L., and Shaw, C.S.J. (2001) Anomalous compression and equation of state of coesite. Physics of the Earth and Planetary Interiors, 124, 71-79.

Bass, J.D., Liebermann, R.C., Weidner, D.J., and Finch, S.J. (1981) Elastic properties from acoustic and volume compression experiments. Physics of the Earth and Planetary Interiors, 25, 140-158.

Bish, D.L. (1993) Rietveld refinement of the kaolinite structure at 1.5 K. Clays and Clay Minerals, 41, 738-744.

Finger, L.W. and Hazen, R.M. (1978) Crystal structure and compression of ruby to 46 kbar. Journal of Applied Physics, 49, 5823.

Jacobsen, S.D., Reichmann, H.-J., Spetzler, H.A., Mackwell, S.J., Smyth, J.R., Angel, R.J., and McCammon, C.A. (2002) Structure and elasticity of single-crystal (Mg,Fe)O and a new method of generating shear waves for gigahertz ultrasonic interferometry. Journal of Geophysical Research, 107, 2037.

Li, B., Rigden, S.M., and Liebermann, R.C. (1996) Elasticity of stishovite at high pressure. Physics of the Earth and Planetary Interiors, 96, 113-127.

Litasov, K.D., Ohtani, E., Ghosh, S., Nishihara, Y., Suzuki, A., and Funakoshi, K. (2007) Thermal equation of state of superhydrous phase B to 27 GPa and 1373 K. Physics of the Earth and Planetary Interiors, 164, 142-160.

Mellini, M. and Zanazzi, P.F. (1989) Effects of pressure on the structure of lizardite-1T. European Journal of Mineralogy, 1, 13-19.

Pacalo, R.E.G. and Weidner, D.J. (1996) Elasticity of superhydrous B. Physics and Chemistry of Minerals, 23, 520-525.

Sinogeiken, S.V., and Bass, J.D. (2000) Single-crystal elasticity of pyrope and MgO to 20 GPa by Brillouin scattering in the diamond cell. Physics of the Earth and Planetary Interiors, 120, 43-62.

Vinograd, V.L., Winkler, B., Putnis, A., Kroll, H., Milman, V., Gale, J.D. and Fabrichnaya, O.B. (2006) Thermodynamics of pyrope-majorite, $Mg_3Al_2Si_3O_{12}$-$Mg_4Si_4O_{12}$, solid solution from atomistic model calculations. Molecular Simulation, 32, 85-99.

Wang, Z., Wang, H., and Cates, M.E. (2001) Effective elastic properties of solid clays. Geophysics, 66, 428-440.

Weidner, D.J., and Carleton, H.R. (1977) Elasticity of coesite. Journal of Geophysical Research, 82, 1334-1346.

Xia, X., Weidner, D.J., and Zhao, H. (1998) Equation of state of brucite: single-crystal Brillouin spectroscopy study and polycrystalline pressure-volume-temperature measurement. American Mineralogist, 83, 68-74.

Yagi, T., Uchiyama, Y., Akaogi, M., and Ito., E. (1992) Isothermal compression curve of $MgSiO_3$ tetragonal garnet. Physics of the Earth and Planetary Interiors, 74, 1-7.

Zou, Y., Irifune, T., Gréaux, S., Whitaker, M.L., Shinmei, T., Ohfuji, H., Negishi, R., and Higo, Y. (2012) Elasticity and sound velocities of polycrystalline $Mg_3Al_2(SiO_4)_3$ garnet up to 20 GPa and 1700 K. Journal of Applied Physics, 112, 014910.